Resonance Raman Spectroelectrochemistry. I. The Tetracyanoethylene Anion Radical

David L. Jeanmaire, Mary R. Suchanski, and Richard P. Van Duyne*

Contribution from the Department of Chemistry, Northwestern University, Evanston, Illinois 60201. Received August 24, 1974

Abstract: A new spectroelectrochemical technique based on the resonance Raman effect is described whereby high resolution vibrational spectra can be obtained for electrogenerated intermediates and products. Both controlled potential coulometric electrolysis in bulk solution and cyclic potential step electrolysis under semiinfinite diffusion mass transport conditions have been tested as electrogeneration modes. Resonance Raman spectra of the tetracyanoethylene anion radical (TCNE·⁻), which exhibits perfectly reversible electrogeneration behavior, have been obtained in both of these electrogeneration modes with 4880, 4765, and 4579 Å Ar⁺ laser excitation. In addition resonance Raman intensity (RRI) vs. time transients produced by single-shot, double-potential steps at a microelectrode have been obtained for the 2194 cm⁻¹ $\nu_1(A_g)$ C≡N and 1421 cm⁻¹ $\nu_2(A_g)$ C=C stretching modes. The Raman transients correlated exactly in time with the corresponding chronoamperometric and transmission chronoabsorptometric signals indicating that the Raman transients and spectra obtained under cyclic potential step conditions result from TCNE·⁻ in the electrochemical diffusion layer.

The elucidation of electrochemical reaction pathways invariably requires the detection, identification, and kinetic monitoring of intermediates and/or products generated either on the electrode surface or in the adjacent solution. It has been demonstrated that spectroscopic monitoring of electrogenerated species (spectroelectrochemistry) is extremely useful for purposes of identification and structural characterization as well as providing superior molecular specificity for detection and kinetic monitoring relative to the usual electrochemical parameters current, potential, time, etc.[1] Restricting discussion to electrogenerated species in solution, the spectroscopic techniques which have made the greatest impact on electrochemistry to date are electron spin resonance[2] (ESR) and electronic absorption spectroscopy[1] (uv-visible). ESR is routinely used for identification of paramagnetic species in bulk solution produced by controlled potential electrolysis and more recently has been applied to quantitative kinetic studies of electrogenerated radical ions in the diffusion layer following current step electrolysis.[3-5] Electronic absorption spectroscopy has proven extremely versatile in that it can be interfaced to electrochemistry in transmission and internal reflection modes at optically transparent electrodes (OTE's) as well as in the specular reflection mode at bulk metal electrodes. In addition uv-visible spectroscopy is readily applied to the most common mass transport conditions including bulk electrolysis,[6] finite diffusion (thin layer electrochemistry),[7] semiinfinite diffusion,[1] and hydrodynamics.[8] The utility of electronic absorption spectroscopy for purposes of species identification is unfortunately limited due to the relatively low information content of uv-visible spectra in fluid solution. However, one finds that because of the high sensitivity of uv-visible spectrophotometric measurements and the large values of electronic absorption extinction coefficients, electronic absorption spectroscopy is most useful for following the kinetics of electrochemical transformations over a wide dynamic range of time from hours to microseconds.

Several attempts have been made to couple vibrational spectroscopy to electrochemistry.[7,9-14] The motivation for this is the greater degree of molecular specificity and sensitivity to subtle environmental factors inherent in vibrational spectroscopy relative to electronic absorption spectroscopy. The attempts made to use infrared spectroscopy (ir) to study electrogenerated species in solution have met with only limited success because of the following experimental limitations: (1) small free spectral window caused by competitive absorption from the solvent/supporting electrolyte

system as well as the electroactive substrate; (2) relatively low spectrophotometric sensitivity due to the small values of infrared extinction coefficients; and (3) rapid time response is limited as a result of the high electrical resistance of infrared transparent electrode materials. Recently it has been suggested that Raman spectroscopy might be more readily applied to electrochemical systems than ir from the viewpoint of free spectral window, ease of cell construction since borosilicate glass will work as a window material, and ease of application to aqueous solutions since water is a poor Raman scatterer.[15,16] The problem with this approach is the lack of sensitivity inherent in the normal spontaneous Raman scattering process. Typically samples must be 0.1–1.0 M in order to get Raman spectra with acceptable signal-to-noise (SN) ratios even for strong Raman scatterers. This lack of sensitivity would appear to preclude the use of ordinary Raman spectroscopy to observe spectra or kinetic transients in solution at the concentration levels of electroactive substrate normally used in electrochemical experiments. Fleischmann and coworkers[17] have, nevertheless, demonstrated that Raman spectroscopy will be very useful for observing strong Raman scatterers adsorbed on high surface area electrodes as a function of applied electrode potential.

In this paper we wish to demonstrate that vibrational spectra of electrogenerated species in bulk solution or in the electrochemical diffusion layer can be readily obtained from solutions originally *ca.* 1×10^{-3} M in electroactive substrate by utilizing the resonance Raman effect.[18] The primary characteristic of resonance Raman spectroscopy that we capitalize on for application to electrochemistry is that laser excitation within an electronic absorption band results in enhancements of the Raman scattering cross section by factors as large as 10^5–10^6 for certain vibrational modes of the electrogenerated species. In addition we will illustrate various advantageous features of resonance Raman spectroelectrochemistry (RRSE) such as: (1) use of low resistance bulk metal electrodes for *in situ* studies in the electrochemical diffusion layer; (2) cell design criteria are relatively unrestrictive from both the Raman spectroscopic and electrochemical points of view; (3) there is essentially no spectral interference from the solvent, supporting electrolyte, or electroactive substrate (unless it is colored); (4) the only requirements for observation of an electrogenerated species by RRSE are that it have a lifetime compatible with its mode of electrogeneration and have an extinction coefficient greater than *ca.* 1000 M^{-1} cm⁻¹ at one (or
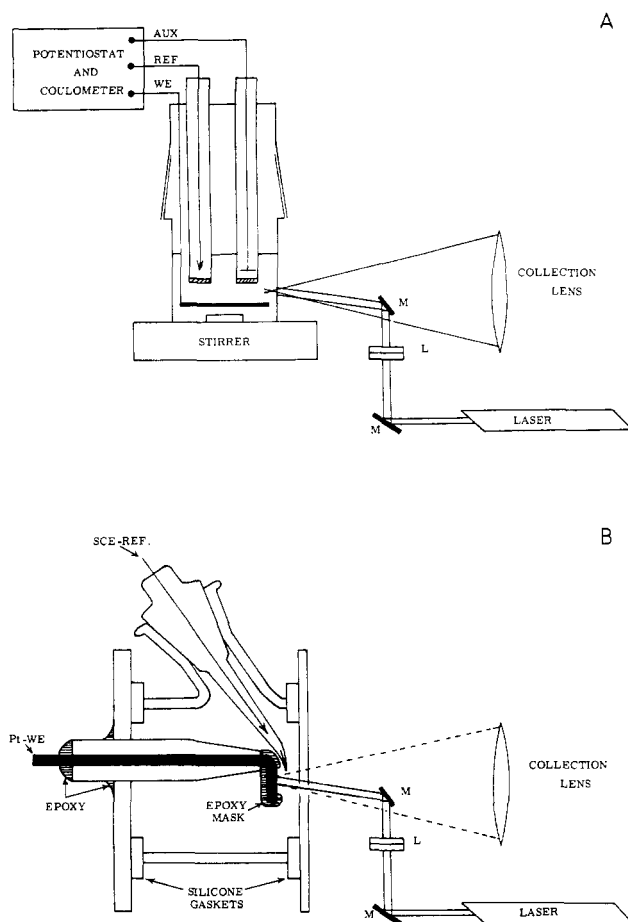
Figure 1. Resonance Raman spectroelectrochemistry cells and backscattering geometry: (A) controlled potential electrolysis cell; (B) "sandwich" cell for semiinfinite diffusion conditions.

more) of the available laser frequencies; and (5) the Raman signals obtained under semiinfinite diffusion cyclic potential step conditions are sufficiently strong to enable resonance Raman intensity (RRI) vs. time transients to be recorded directly in a single-shot, double-potential step experiment on the 1–5 sec time scale.

To illustrate these features of RRSE, the electroreduction of tetracyanoethylene (TCNE) to its anion radical (TCNE·⁻) was chosen. This choice was based on literature data which indicated that: (1) TCNE·⁻ was a relatively stable anion radical when prepared chemically; (2) the TCNE + e⁻ ⇌ TCNE·⁻ reaction was electrochemically reversible as judged from AC and DC polarographic criteria; (3) some ir and Raman vibrational data were available for comparison; and (4) the electronic absorption spectrum of TCNE·⁻ showed acceptable, although not optimum, overlap with the Ar⁺ laser lines.

Experimental Section

Cyclic voltammetry and double-potential-step chronoamperometry were performed in a nitrogen degassed, low volume (10 ml), three-electrode cell previously described in connection with low-temperature electrochemical studies.[19] Controlled potential reversal coulometry was carried out in the nitrogen degassed, three-compartment cell pictured schematically in Figure 1A. The reference electrode was an SCE connected to the cell via a salt bridge containing solvent and supporting electrolyte only. A platinum foil served as the auxilliary electrode and a 10 cm² platinum gauze formed the working electrode. The solutions in the auxiliary and reference electrode compartments were separated from the working electrode solution by 10 mm medium porosity, sintered glass frits. For coulometry experiments involving more rigorous exclu-

sion of atmospheric oxygen than provided by the usual nitrogen deoxygenation procedure, a three-compartment vacuum electrolysis cell was used. The vacuum cell is similar in basic design to the cell in Figure 1A except that a silver wire quasi-reference electrode (QRE) separated from the electrolysis solution by a platinum wire leak junction and freeze–pump–thaw degassing were used. Separate potentiostats were employed for transient electrochemical experiments and bulk electrolysis. The potentiostat for cyclic voltammetry and potential step work was of conventional operational amplifier design[20] (Philbrick Model 1024's for control and current measuring amplifiers and Model 1026 for the voltage follower) and provided for input voltage offset and positive feedback iR drop compensation. A Hewlett-Packard Model 3300 function generator provided triangular and potential step input waveforms for the potentiostat. A Hewlett-Packard Model 7004B X-Y recorder and a Tektronix Model 564 storage oscilloscope were used for all transient electrochemistry signal monitoring purposes. The potentiostat for controlled potential electrolysis was of similar design but configured around a Kepco operational power supply (±36 V compliance and 1.5 ampere output) acting as the control amplifier. A self-contained initial voltage source, iR drop compensation, and cell current integration were also available on this instrument. The integrator output signal (coulombs vs. time) was monitored with a Keithley Model 160 digital multimeter and a Houston Instruments Model 3000 strip chart recorder.

Transient electronic absorption spectroelectrochemical measurements were performed at fixed wavelengths with an apparatus consisting of a 55-Watt quartz–iodide–tungsten lamp, Kepco Model BKF-12-7 lamp power supply, a Bausch and Lomb high intensity monochromator fitted with a Model 33-88-02 grating, and an EMI Model 6256B photomultiplier (PMT) mounted in a Pacific photomultiplier housing. These components were assembled in a light tight "black box" configuration similar to that previously described by Winograd and Kuwana.[21] The cell used for transmission spectroelectrochemistry was of the "sandwich" type[1] and used a vapor deposited platinum film optically transparent electrode (Pt-OTE). The potentiostat described above for cyclic voltammetry was used for the potential step chronoabsorptometry measurements.

Resonance Raman spectra were obtained using a 0.85 m Spex Model 1401 double monochromator with standard photon counting detection. The PMT used for Raman work was a thermoelectrically cooled RCA C31034. A light stabilized Spectra Physics Model 164 argon ion laser operating in the 10–200 mW incident power range was employed for all RRSE experiments. Laser power measurements were made with a Coherent Radiation Model 210 power meter. The oblique backscattering geometry used in RRSE with the nitrogen deoxygenated, controlled potential electrolysis cell is illustrated in Figure 1A. A cylindrical lens, L, (90 mm focal length) and a small front surface mirror, M, mounted above L are combined to produce a slit-shaped illuminated region in the controlled potential electrolysis cell. The Raman scattered light from this illuminated region can now be efficiently focused onto the spectrometer slit with an f 1.6 collection lens. For semiinfinite diffusion electrogeneration conditions, a modified version of the "sandwich" type cell used for conventional spectroelectrochemistry with Pt-OTE's was devised. A cross-sectional view of this cell along with the backscattering optics is shown in Figure 1B. Not pictured for the sake of clarity in Figure 1B are the nitrogen inlet and outlet ports, platinum wire coil auxiliary electrode which is coaxial with the post mounting the 10 gauge platinum wire working electrode (Pt-WE), and the exterior aluminum clamp which compresses the front and back glass plates against the silicone rubber gaskets (General Electric RTV-112) and the cell body to make a solution tight seal. The cell is sealed in various places with a solvent resistant epoxy resin (Varian Associates Torr-Seal®). This epoxy is also used to mask the Pt-WE to an active rectangular area of 1 × 4 mm. Before applying the epoxy mask the Pt-WE was ground to a hemispherical cross-section and polished to a mirror finish with 600 grit Al₂O₃ in order to make a good approximation to a planar working electrode. Focusing the Raman light scattered from the working electrode onto the spectrometer slit is an extremely critical operation. Consequently this cell is mounted on an X-Y-Z-θ micropositioner to permit precise location of the Pt-WE with respect to the laser beam deflection mirror, collection lens, and monochromator slit. All Raman spectra were recorded on
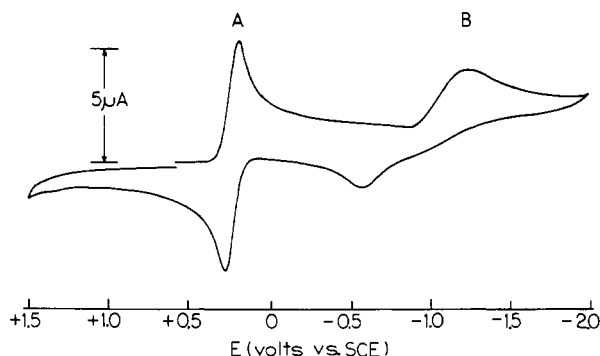
Figure 2. First-scan cyclic voltammogram of 0.90 mM TCNE in acetonitrile containing 0.10 M TBAP at a Pt disk microelectrode. The scan rate = 0.200 V sec.$^{-1}$

magnetic tape using a 1.00-sec counting interval, processed by the CDC 6400 computer, and plotted on a Calcomp plotter. Resonance Raman intensity (RRI) vs. time transients were obtained by applying a single-shot, double-potential step to the Pt-WE using the cyclic voltammetry potentiostat and recording the analog output of the ratemeter, which monitors the Raman signal, on the Hewlett-Packard Model 7004 B X-Y recorder fitted with a Model 17172A time base.

TCNE was purchased from Aldrich and purified by two vacuum sublimations at ca. 100°. Spectroquality acetonitrile from Burdick and Jackson Laboratories (uv cutoff 189 nm) was dried using the activated alumina technique.[19,22] Tetra-n-butylammonium perchlorate (TBAP) and tetra-n-ethylammonium perchlorate (TEAP) were used as supporting electrolytes as supplied by Southwestern Analytical Chemicals. The TBAP and TEAP were thoroughly dried in vacuo and stored over P_2O_5 in a vacuum desiccator prior to use. All other chemicals were reagent grade and all solutions were deoxygenated by nitrogen bubbling unless otherwise specified.

Results and Discussion

Electrochemical Behavior of TCNE. The cyclic voltammetry of TCNE in acetonitrile solution is shown in Figure 2. Scanning in the cathodic direction, peaks due to the generation of TCNE·$^-$ (peak A, E_{pc} = +0.207 V vs. SCE at a scan rate of 0.200 V sec^{-1}) and TCNE^{2-} (peak B, E_{pc} = -1.18 V vs. SCE at a scan rate of 0.200 V sec^{-1}) are observed. The results of a cyclic voltammetry scan rate study for the TCNE/TCNE$^-$ wave are listed in Table I. The constancy of $i_{pc} V^{-1/2} C^{0-1}$ and the essential invariance of i_{pa}/i_{pc} = 1.00 ± 0.02 with scan rate are indicative of the chemical stability of electrogenerated TCNE·$^-$ on this time scale.[23] The electrogeneration of TCNE·$^-$ also appears to be electrochemically reversible (fast heterogeneous electron transfer rate constant) since at low scan rates the ΔE_p approaches the theoretical value of 60 mV for a one-electron transfer. The monotonic increase of ΔE_p with scan rate is caused by residual uncompensated iR drop. In contrast the electrogeneration of the dianion appears to be electrochemically quasireversible since the peak separation is greater than 620 mV for all sweep rates tested and furthermore ΔE_p increases substantially with scan rate. This increase was not studied quantitatively but we can report that ΔE_p is 800 mV at a scan rate of 0.300 V sec^{-1}. This increase is far too large to be accounted for by iR drop in view of the internal calibration of this effect provided by the first wave. The oxidation wave at -0.55 V vs. SCE in Figure 2 is correlated with peak B and indicates that the dianion exhibits significant chemical stability on the time scale of a few seconds. It is tempting to speculate that the cause of the quasireversible electron transfer to form the dianion is due to a geometry change and that TCNE^{2-} is a nonplanar species. The control of heterogeneous charge transfer rates by conformational changes has been observed in the reduction of

nonplanar cyclooctatetraene to its planar anion radical.[24] The chemical reversibility of the TCNE + e$^-$ ⇌ TCNE·$^-$ electrode reaction has been further demonstrated by double-potential step chronoamperometry experiments in which the potential was stepped from +0.60 V vs. SCE to -0.20 V vs. SCE. Over a range of forward step times from 0.10 ≤ τ ≤ 2.50 sec, the current ratio $i_a(2 \tau)/i_c(\tau)$ was found to be 0.30 ± 0.01 as compared to the theoretical value 0.2929 of this parameter for a perfectly reversible (i.e., no followup chemical reactions) system.[25]

The long term stability of electrogenerated TCNE·$^-$ was evaluated by controlled potential reversal coulometry in bulk solution.[26] The coulometry parameters n_{app} (number of Faradays consumed per mole of TCNE) and Q_b/Q_f are listed in Table II as a function of the bulk TCNE concentration. These results demonstrate that the reduction of TCNE is a clean one-electron transfer and that electrogenerated TCNE·$^-$ is stable in this medium for at least 40 min (twice the forward electrolysis time). Coulometry experiments were also carried out in which TCNE·$^-$ was generated over a period of 20 min; the cell was then left at open circuit for 1.5 hr to simulate the time period required to scan a resonance Raman spectrum at 25 cm^{-1} min^{-1} over the range 100 to 2500 cm^{-1}, and then TCNE·$^-$ was oxidized back to TCNE. In experiments of this type Q_b/Q_f ratios in the range 0.85 to 0.95 were typically found indicating that there is a slow decay reaction of TCNE·$^-$. This decay reaction was traced to residual O_2 in the cell or O_2 that diffused

Table I. Cyclic Voltammetry Results for TCNE + e$^-$ ⇌ TCNE·$^{-a}$

Scan rate, V sec.$^{-1}$	$i_{pc}/(V^{1/2}C^0)$	i_{pa}/i_{pc}	ΔE_p, mV
0.050	14.5	0.98	62
0.075	14.4	0.99	69
0.100	14.1	1.00	71
0.125	14.2	1.00	72
0.150	14.2	1.00	75
0.175	14.4	1.00	77
0.200	14.4	0.98	77
0.225	14.3	0.99	79
0.250	14.3	0.99	80
0.275	14.3	0.99	83
0.300	14.3	1.00	84
0.325	14.3	1.00	86
0.350	14.1	1.01	90
0.375	14.1	1.01	90
0.400	14.1	1.01	92
0.425	14.1	1.01	95
0.450	14.0	1.02	98
0.475	14.1	1.01	100
0.500	14.1	1.02	102

^{a}The solution was 0.90 mM TCNE and 0.10 M TBAP in CH$_3$CN. The voltage limits were +0.60 V vs. SCE to -0.20 V vs. SCE. i_{pc} = peak cathodic current; ΔE_p = $|E_{pc} - E_{pa}|$; i_{pa} = peak anodic current; C^0 = bulk concentration of TCNE.

Table II. Controlled Potential Coulometry Results for TCNE + e$^-$ ⇌ TCNE·$^{-a}$

[TCNE], mM	$n_{app}{}^b$	$Q_b/Q_f{}^{b,c}$
0.23	1.01	1.00
0.46	1.00	0.99
0.75	0.91	0.98
1.00	1.00	0.93
1.50	0.96	0.98
1.94	0.95	0.97
3.00	1.00	0.97

^{a}In 0.1 M TBAP/CH$_3$CN; deoxygenated by nitrogen bubbling. ^{b}Average of two replicates at each concentration. $^c Q_f$ = charge accumulated in reduction of TCNE at -0.20 V vs. SCE. Q_b = charge recovered in oxidation of TCNE·$^-$ at +0.60 V vs. SCE. Duration of forward electrolysis = 20 min.

Table III. Spectroelectrochemically Determined $\epsilon(\lambda)$ for TCNE·$^{-a}$

λ, nm	A (t = 1.00 sec)^b	$\epsilon(\lambda) \times 10^{-3}$,^{c} M^{-1} cm^{-1}	$\epsilon(\lambda) \times 10^{-3}$,^{d} M^{-1} cm^{-1}
350	0.008	1.4	
366	0.014	2.5	2.4
375	0.018	3.2	3.07
382	0.022	3.8	3.81
390	0.026	4.7	4.66
398	0.032	5.7	5.46
407	0.034	6.2	6.20
416	0.042	7.5	6.89
425	0.040	7.1	7.10
435	0.042	7.5	7.10
445	0.039	6.9	6.52
450	0.032	5.7	
457	0.033	5.9	5.67
468	0.024	4.3	4.40
475	0.012	2.2	
485	0.005	0.9	

^{a} Monochromator bandpass varied from 1 to 3 nm over the spectral range 500 to 350 nm. ^{b} The solution was 1.00 mM TCNE and 0.1 M TBAP in CH$_3$CN. The corresponding value of i (t = 1.00 sec) was 38.5 × 10^{-6} A. ^{c} Calculated from eq 3. Electrode area = 0.15 cm^2. Estimated error limits for $\epsilon(\lambda)$ are no worse than $\epsilon(\lambda) \times 10^{-3}$ = ±0.2. ^{d} Reference 28.

Figure 3. TCNE·$^-$ electronic absorption spectrum in 0.1 M TBAP-acetonitrile solution from 350 to 550 nm. Solid line, absorption spectrum obtained for TCNE·$^-$ prepared by vacuum electrolysis. Points, transient spectrum (1.00-sec generation time) determined by potential-step chronoabsorptometry. Arrows, position of Ar$^+$ laser lines used in obtaining resonance Raman spectra of TCNE·$^-$.

into the cell over these long time periods. It is unlikely that TCNE·$^-$ reacts with O_2 by the usual electron transfer mechanism for radical anion decay because the E^0 for TCNE·$^-$ formation is at least 1.0 V positive of that for O_2·$^-$ formation.[27] Webster[28] has previously reported that O_2 reacts with K$^+$TCNE·$^-$ in acetonitrile solution when it is bubbled through for 0.5 hr to form 36 and 22% yields of potassium tricyanoethenolate and potassium pentacyanopropenide, respectively. Presumably 42% K$^+$TCNE·$^-$ remains. The mechanism of this reaction does not appear to have been investigated in any detail.

The electrochemical results presented here conclusively demonstrate that TCNE·$^-$ can be electrogenerated and will remain stable both for transient and long term resonance Raman spectroelectrochemistry experiments provided that care is taken to exclude atmospheric O_2.

Electronic Absorption Spectroelectrochemistry of TCNE·$^-$. Since the resonance Raman effect involves excitation within an electronic absorption band, it is essential to characterize the electronic absorption spectrum of the species to be studied via resonance Raman spectroscopy. A potential problem exists in this connection for RRSE in particular and in general for the study of potentially unstable intermediates such as radical ions by resonance Raman spectroscopy. If the species of interest partially or fully decays during the time period required to scan the Raman spectrum and the decay products absorb substantially at the laser excitation wavelength, one may observe either a mixed spectrum of the intermediate and product or only the product spectrum. If this situation exists and the objective of the experiment is to provide fundamental information on the vibrational frequencies of the intermediate, a spectral interpretation problem clearly arises. On the other hand, RRSE would be useful in identifying the decay product in this situation. In view of this possibility and the slow decay reaction of TCNE·$^-$ with O_2 noted above, experiments were carried out to characterize the electronic absorption spectrum of TCNE·$^-$ under the electrogeneration conditions to be used for resonance Raman spectroelectrochemical studies.

On the 0–10-sec time scale, the electronic absorption spectrum of TCNE·$^-$ electrogenerated in nitrogen deoxygenated CH$_3$CN solution was obtained by potential step, transmission spectroelectrochemical measurements at a se-
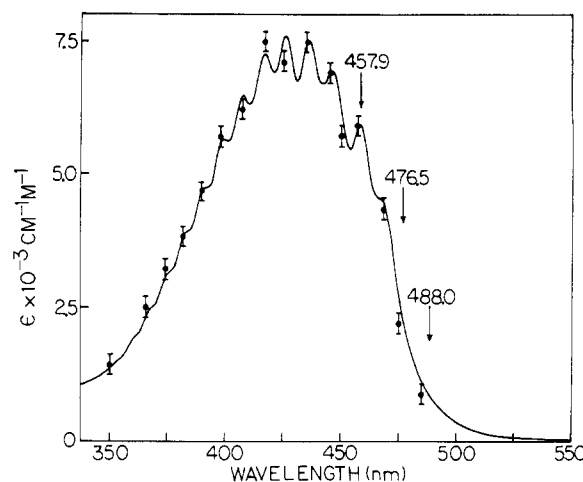
ries of fixed wavelengths using a Pt-OTE. The potential of the Pt-OTE was stepped from +0.60 V vs. SCE to −0.20 V vs. SCE for a duration of 1.00 sec and returned to the initial potential. During the potential step, simultaneous current-time and absorbance–time transients were recorded by an online digital computer (Raytheon 704) interfaced to the spectroelectrochemical apparatus. For a perfectly reversible electrochemical system, the forward step of the current-time transient is quantitatively described by the Cottrell equation

$$i(t) = nFAD^{1/2}C^0(\pi t)^{-1/2} \qquad (1)$$

and that of the absorbance–time transient by[21]

$$A(t, \lambda) = 2\pi^{-1/2}\epsilon(\lambda)C^0(DT)^{1/2} \qquad (2)$$

In eq 1 and 2, n is the number of electrons transferred, F is the Faraday, A is the area of the Pt-OTE, D is the diffusion coefficient of TCNE, C^0 is the bulk concentration of TCNE, t is the elapsed time into the potential step electrolysis, and $\epsilon(\lambda)$ is the extinction coefficient of TCNE·$^-$ at wavelength λ. Dividing eq 2 by eq 1 cancels out D and C^0; rearrangement gives

$$\epsilon(\lambda) = \frac{nFA}{t}\left[\frac{A(t,\lambda)}{i(t)}\right] \qquad (3)$$

Taking the area of the Pt-OTE as the geometric area of its mask (0.15 cm^2) and using matched $A(t,\lambda)$ and $i(t)$ data at t = 1.00 sec, the extinction coefficients reported in Table III were calculated from eq 3. As shown in Table III the correspondence between the spectroelectrochemically measured $\epsilon(\lambda)$ and the conventionally measured $\epsilon(\lambda)$ reported by Webster is quite good. The extinction coefficient data are also plotted as a 1.0-sec duration transient absorption spectrum in Figure 3.

Further evidence for the stability of TCNE·$^-$ on the time scale of a few seconds in nitrogen-degassed acetonitrile is obtained from the double-potential-step chronoabsorptometric response. The phenomenological theory of double-potential-step chronoabsorptometry predicts that the ratio $[A(2\tau) - A(\tau)]/A(\tau) = 0.586$,[21] where τ is the duration of the potential step, for a perfectly reversible system. In all of the experiments used to obtain the transient absorption spectrum in Figure 3, the double-potential step absorbance

ratios were 0.57 ± 0.02. For those transients with high signal-to-noise ratios at the maximum of the absorption spectrum, the double potential step absorbance ratios were found to be 0.582 ± 0.003 for replicate experiments.

On the controlled potential electrolysis time scale, the electronic absorption spectrum of TCNE·⁻ was obtained by carrying out an electrolysis under vacuum line conditions to ensure the exclusion of oxygen. The acetonitrile used to prepare the electrolysis solution was degassed by four freeze-pump-thaw cycles (10^{-3} Torr) and transferred by distillation to a previously evacuated electrolysis cell containing TBAP and TCNE. TCNE·⁻ was coulometrically generated at −0.20 V. vs. Ag wire QRE to ca. 90% completion after which the cell was disconnected from the vacuum line and 0.5 ml of the electrogeneration solution was poured into a side arm of the cell containing an optical cell. The TCNE·⁻ solution in the optical cell was diluted by distilling approximately 5 ml of CH₃CN into the side arm from the main electrolysis solution. The absorption spectrum of this diluted solution is shown in Figure 3 where it has been normalized at 435 nm to the spectroelectrochemically determined extinction coefficient. The agreement between the spectrum obtained under vacuum electrolysis conditions and the transient spectrum is excellent. In addition both spectra agree well with the Na⁺TCNE·⁻ spectra reported by Webster in acetonitrile solution[28] and by Itoh in 2-methyltetrahydrofuran solution.[29] The electronic absorption spectrum of TCNE·⁻ obtained under nitrogen deoxygenation controlled potential electrolysis conditions and anaerobic transfer to the optical cell is virtually identical to that shown in Figure 3 except that the absorbance at the 416 nm vibrational maximum is slightly greater than that at the 425 nm maximum. On standing, the absorbance at 416 nm decays by a factor of 2 in a 3.0-hr period to give a differently shaped spectrum with absorption maxima at 416 and 398 nm and a low absorbance tail showing some structure in the 440–500-nm range. Presumably this decay is the result of the slow TCNE·⁻ + O₂ reaction.

Resonance Raman Spectroelectrochemistry of TCNE·⁻. Two electrogeneration modes have been developed and tested for use in RRSE experiments: (1) controlled potential coulometric electrolysis in bulk solution and (2) cyclic potential-step electrolysis at a microelectrode where semiinfinite diffusion mass transport conditions prevail.

The controlled potential coulometry electrogeneration mode involves a macro-scale electrolysis which if carried to completion results in the quantitative conversion of electroactive substrate to electrode reaction product(s). Typical initial concentrations of the substrate are 10^{-4} to 5×10^{-3} M and require electrolysis times of 100 sec to several hours depending on the coulometry cell design, potentiostat compliance, and efficiency of convective mass transport. The role of the electrode in this type of experiment is solely to act as a controlled E^0 oxidizing or reducing agent. Several means of examining the resulting electrolysis solution by resonance Raman spectroscopy have been evaluated. A sample of the electrolysis solution can be transferred from the cell to an appropriate Raman sample tube and illuminated statically in 90° geometry or mounted in a spinner and illuminated in backscattering geometry.[30] It has been well documented in the Raman literature that moving the sample relative to the exciting laser beam is very advantageous for optically dense samples since it prevents solution boiling and/or sample decomposition by dissipating the laser energy over a larger sample area. This feature can be incorporated for electrogenerated samples and the necessity for transferring the electrolysis solution to a separate sample cell eliminated by fitting the controlled potential electrolysis cell with a recirculating pump (centrifugal type,
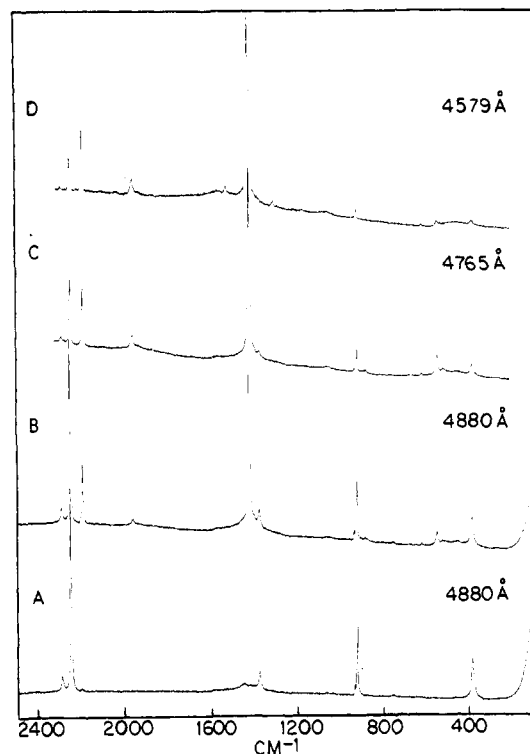

Figure 4. Resonance Raman spectra of TCNE·⁻ electrogenerated by controlled potential coulometry at −0.20 V vs. SCE in 0.1 M TBAP/CH₃CN: (A) background scan [TCNE] = 2.1 mM, cell at open circuit, laser power = 106 mW, bandpass = 2.0 cm⁻¹; (B) [TCNE·⁻] = 2.1 mM, laser power = 106 mW, bandpass = 2.1 cm⁻¹; (C) [TCNE·⁻] = 3.3 mM, laser power = 80 mW, bandpass = 2.1 cm⁻¹; (D) [TCNE·⁻] = 3.3 mM, laser power = 30 mW, bandpass = 2.3 cm⁻¹. All spectra were scanned at 50 cm⁻¹ min⁻¹ using a 1.00-sec counting interval per unit wavenumber increment. Plasma lines have been manually removed from the spectra excited at 4765 and 4579 Å.

Cole-Parmer Model 7004-62). The electrolyzed solution containing the species to be studied is pumped through a 2 mm i.d. borosilicate glass tube, located at the entrance optics of the Raman spectrometer, and back to the electrolysis cell. Although this configuration works adequately, a simpler and more widely applicable configuration involves backscattering the laser beam directly from the glass electrolysis cell (see Figure 1A). The stirring action normally required to establish efficient convective mass transport in the electrolysis cell provides sufficient motion to prevent local heating or sample decomposition. This backscattering arrangement has proved eminently satisfactory in that it places no special requirements either electrochemical or optical on the cell design, is readily applied to vacuum electrolysis cells, and as a result is advantageous when air sensitive solutions (for example, radical anions) are involved. Consequently all of the resonance Raman spectra presented in this paper using the controlled potential coulometry electrogeneration mode have been obtained with the backscattering configuration.

Figure 4A shows the normal Raman spectrum of an acetonitrile solution containing 2.1 mM TCNE and 0.1 M TBAP. All bands in this spectrum are due to acetonitrile[31] with the exception of the 931 cm⁻¹ $\nu_1(A_1)$ Cl–O stretch of ClO₄⁻.[32] No bands are observed for TCNE since the concentration is too low for normal Raman bands to be seen and there is no electronic absorption band which overlaps with the Ar⁺ laser lines so that no resonance enhancement can be observed. Apparently no Raman features in the 100 to 2500 cm⁻¹ region are contributed by the tetrabutylammonium cation. The fluorescence background count rate of

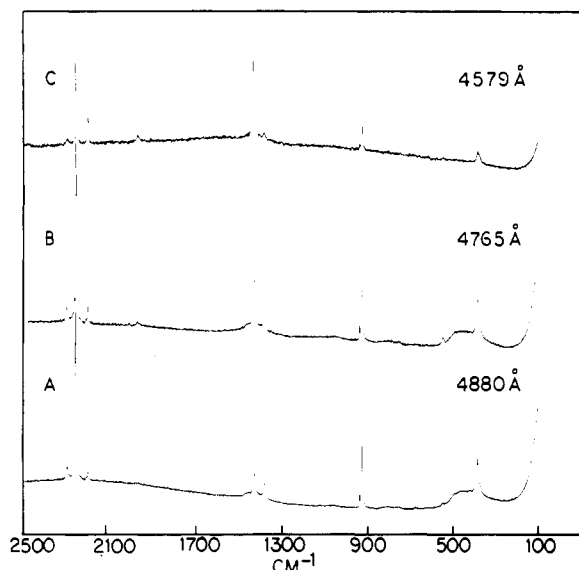**Figure 5.** Resonance Raman spectra of TCNE·⁻ electrogenerated by cyclic potential step electrolysis at a rectangular Pt microelectrode in 4.0 mM TCNE/0.1 M TEAP/CH$_3$CN. The potential-step limits were +0.60 V vs. SCE and −0.20 V vs. SCE and the step frequency was 10.0 Hz. (A) laser power = 160 mW, bandpass = 2.0 cm⁻¹; (B) laser power = 150 mW, bandpass = 2.1 cm⁻¹; (C) laser power = 15 mW, bandpass = 2.3 cm⁻¹. All spectra were scanned at 50 cm⁻¹ with a 1.00-sec counting interval per unit wavenumber increment. Plasma lines have been manually removed from the 4765- and 4579-Å spectra.

the solvent-supporting electrolyte solution was found to vary over the range 2,000 to 12,000 Hz (at 2500 cm⁻¹, 2–3 cm⁻¹ bandpass, and ca. 100 mW of 4880-nm laser power) depending on the source and drying treatment of the TBAP. More rigorous supporting electrolyte purification and handling techniques will have to be developed for RRSE work in order to reproducibly obtain the low fluorescence backgrounds exhibited by the solutions in Figure 4. Figures 4B, 4C, and 4D show typical Raman spectra obtained from TCNE solutions electrolyzed at −0.20 V vs. SCE and excited with the Ar⁺ laser 4880, 4765, and 4579 Å lines, respectively. The location of these laser lines with respect to the vibrational fine structure maxima in the electronic absorption spectrum of TCNE·⁻ is shown in Figure 3. None of these lines are coincident with the absorption maximum of TCNE·⁻ so that perhaps the spectra in Figure 4 should be more properly termed preresonance Raman spectra. The main vibrational features observed in the electrolyzed TCNE solutions excited at 4880 Å are at 540, 1421, 1961, and 2194 cm⁻¹. Very weak bands at ∼615 and ∼970 cm⁻¹ are also observed. These are tentatively assigned to as yet unidentified products of the TCNE·⁻ + O$_2$ decay reaction since their appearance correlated with low Q_b/Q_f ratios. The four main vibrational features are also observed when TCNE·⁻ is excited at 4765 Å and are more strongly resonance enhanced as judged by the intensities of the TCNE·⁻ bands relative to the nearest solvent band. The ∼615 and ∼870 cm⁻¹ (decay product?) peaks are also evident. With 4579-Å excitation we find the 1421, 1961, and 2194 cm⁻¹ bands still more strongly resonance enhanced than with 4880 and 4765 Å excitation; however, it appears that the 540-cm⁻¹ band has moved out of resonance since it is less strongly enhanced than at 4765 Å. Two new weak bands at 1306 and 1565 cm⁻¹ are evident with the 4579-Å excitation. These are also assigned to TCNE·⁻ decay product(s).

In the cyclic potential-step mode of electrogeneration, a square voltage waveform is applied to a small area (<1 cm²) working electrode in an unstirred solution. The only mass transport process operative in bringing electroactive

material from the bulk of solution to the electrode surface is diffusion. The voltage limits of the square wave are chosen so as to form the electrode reaction product at a diffusion-controlled rate on the forward step and to form reactant at a diffusion controlled rate on the reverse step. This requires the voltage limits to be set at least 60/n mV past the corresponding E_p in the cyclic voltammogram.[23] For the TCNE electrode reaction, the limits of +0.60 and −0.20 V vs. SCE were chosen. The frequency of the applied square wave used in the experiments reported here was 10 Hz. The choice of this frequency is somewhat arbitrary although it should be considerably faster than the time constant of the ratemeter or the counting time interval at fixed wavelength to prevent the Raman spectrum from being modulated by the electrochemical generation. We have successfully obtained Raman spectra using step frequencies as high as 500 Hz. Using this approach steady state concentration profiles of TCNE·⁻ and TCNE are set up near the electrode surface. This concentration distribution of TCNE·⁻ is excited by backscattering the excitation laser beam directly from the polished platinum electrode surface at an oblique angle (see Figure 1B) and the Raman spectrum is scanned in a conventional manner. A typical scan rate is 50 cm⁻¹ min⁻² so for the 100 to 2500 cm⁻¹ range covered in the TCNE·⁻ studies a total square wave electrolysis time of about 25 min is involved.

Raman spectra of TCNE·⁻ generated by cyclic potential steps (10 Hz) and excited at 4880, 4765, and 4579 Å are shown in Figure 5. The TCNE·⁻ vibrational modes at 540, 1421, 1961, and 2194 cm⁻¹ are clearly seen in all of these spectra. The additional weak bands at ∼615, ∼870, 1306, and 1565 cm⁻¹ seen in the controlled potential coulometry spectra are not seen in the cyclic potential step spectra. The absence of these bands could be due to the lower S/N ratio of the cyclic potential step spectra as compared to the controlled potential coulometry spectra. A more probable explanation in view of our cyclic voltammetry, double-potential-step chronoamperometry, and double-potential-step chronoabsorptometry data which demonstrate the stability of TCNE·⁻ over periods at least as long as 5.00 sec is that during the "on" time of the 10-Hz cyclic square wave (0.050 sec) there is insufficient time for TCNE·⁻ to react with O$_2$ or other scavengers to generate significant decay product concentrations in the electrochemical diffusion layer. Thus we regard the 540, 1421, 1961, and 2194 cm⁻¹ bands *only* as representing the resonance Raman spectrum of TCNE·⁻ at these laser excitation wavelengths. It should be noted that no degradation in any electrochemical response could be detected for the TCNE solutions after they had been subjected to cyclic potential step electrolysis for the duration of the Raman scan (ca. 1 hr).

The main vibrational features of the TCNE·⁻ resonance Raman spectra presented in Figures 4 and 5 can be interpreted by analogy with the assignments made by Devlin[33] for TCNE·⁻ in the solid state prepared by condensation of TCNE and alkali metal vapors at −180°. Thus the 540, 1421, 1961, and 2194 cm⁻¹ bands observed by RRSE are assigned as the ν_3(A$_g$) C–C symmetric stretch, the ν_2(A$_g$) C=C symmetric stretch, a $\nu_2 + \nu_3$ combination band, and the ν_1(A$_g$) C≡N symmetric stretch, respectively. These assignments are summarized in Table IV along with a portion of the Raman vibrational data from the literature for TCNE, Na⁺TCNE·⁻, K⁺TCNE·⁻, and the charge transfer complexes of TCNE with benzene, toluene, and m-xylene.

The Raman spectrum of TCNE neutral obtained in the course of this work is an excellent match to spectra previously reported in the literature. The comparison of the solution phase TCNE·⁻ resonance Raman spectrum obtained by RRSE with the solid state work of Devlin permits several interesting observations to be made. In the solution

Table IV. Comparative Raman Vibrational Data for TCNE Systems

Assign	I TCNE,[a] cm⁻¹	II TCNE,[b] cm⁻¹	III K⁺ TCNE·⁻,[c] cm⁻¹	IV Na⁺ TCNE·⁻,[c] cm⁻¹	V $(C_4H_9)_2N^+$ TCNE·⁻,[d] cm⁻¹	VI TCNE– benzene,[e] cm⁻¹	II–V Δν, cm⁻¹	I[e]–VI Δν, cm⁻¹
ν_1 [a,c]	2231, 2226[e]	2231	2215[f]	2225		2223		+3
			2185[f]	2188	2194		+37	
$\nu_2 + \nu_3$ [c]			1960		1961			
			1900	1910				
ν_2 [a,c]	1566, 1570[e]	1562	1420	1430	1421	1565	+141	+5
			1365	1380				
$2\nu_3$ [c]				1050				
ν_3 [c]	535	533	540	530	540		−7	
			525	523				

[a] R. A. Miller et al., *Spectrochim. Acta*, **20**, 1233 (1964). In acetone or CH_3NO_2 solution. [b] This work, solution in CH_3CN, 5145-Å excitation. [c] Reference 33. [d] This work, electrogenerated in CH_3CN, 4880-, 4764-, and 4579-Å excitation. [e] Reference 34. Toluene and *m*-xylene complexes give identical frequencies. [f] Solid state splitting.

TCNE·⁻ spectra no vibrational features other than the ν_3 mode are observed in the 100 to 1400 cm⁻¹ region which supports Devlin's assignment of the intense, low frequency band near 160 cm⁻¹ to a lattice librational mode (ν_L) rather than to an intrinsic feature of isolated TCNE·⁻ such as the low-frequency fundamental $\nu_5(A_g)$ which is calculated to be near 130 cm⁻¹. This statement applies to the ν_L overtones observed in solid state TCNE·⁻ as well. Another characteristic feature of the solid state spectra which is absent in our solution spectra is splitting caused by dynamic coupling of either the factor group or transverse/longitudinal (T/L) type in ν_1, ν_2, ν_3, and $\nu_2 + \nu_3$. Except for the C≡N stretch the solution frequencies correspond to the high frequency, resonance enhanced component of the solid state splitting. This may be possible evidence in support of assigning the splitting to the T/L type. Of particular interest is the observation of the $\nu_2 + \nu_3$ combination band in the RRSE experiments but no overtones of any of the resonance enhanced fundamentals could be observed in contrast to the solid state case where both $\nu_2 + \nu_3$ and $2\nu_3$ were found. The observation of high intensity combination bands and overtones is usually considered to be the distinguishing feature of resonance from preresonance Raman scattering. The TCNE·⁻ spectra in Figures 4 and 5 may indeed be resonance spectra if ν_3, which is also very weak in the TCNE neutral spectrum, was sufficiently weak so that $2\nu_3$ could not be observed but "borrowed" sufficient intensity in its combination with the very strongly resonance enhanced ν_2 to permit its observation as a combination band.

Comparison of the vibrational frequency shifts of a radical ion with respect to its neutral is one important type of chemical information that can be provided by RRSE studies. More accurate frequency shifts between TCNE and TCNE·⁻ can be determined from our RRSE data since the ambiguity caused by the solid state splitting of the fundamentals is removed. This will become quite important when frequency shifts on the same order as the solid state splitting are to be interpreted. The frequency shifts obtained in this work are shown in Table IV. They are in the same direction and are of the same general magnitude as those found by Devlin for $\Delta\nu_1$ and $\Delta\nu_2$; however, $\Delta\nu_3 = (\nu_3^{neutral} - \nu_3^{anion})$ appears to be +3 cm⁻¹ from the data in Tables II and III of ref 33; whereas, we find $\Delta\nu_3 = -7$ cm⁻¹ which is in better agreement with the prediction based on simple Hückel MO bond orders that addition of the extra electron to the lowest TCNE antibonding MO increases the C–C bonding character. One other possible application of frequency shift measurements will be to monitor the extent of electron transfer in electron donor–acceptor (EDA) complexes. From the data presented in Table IV, we would conclude that there is very little net electron transfer in the EDA complexes of TCNE–benzene, TCNE–toluene, and TCNE-*m*-xylene studied by Kaya et al.[34] since the ν_1 and ν_2 vibrational frequencies in the complex are much more similar to those of TCNE neutral than TCNE anion. Further work is needed to determine the extent to which vibrational frequency shifts are valid monitors of the degree of electron transfer in EDA complexes.

One of the most valuable features of electronic absorption spectroelectrochemistry is that absorbance vs. time transients can be measured which provide the opportunity to monitor the decay kinetics of a transient species in the electrochemical diffusion layer.[1] Only recently has this capability been demonstrated for in situ ESR spectroelectrochemistry.[3-5] The possibility of obtaining resonance Raman intensity (RRI) vs. time transients for the individual vibrational modes of an electrogenerated species in the diffusion layer was tested by setting the wavelength of the double monochromator to a resonance Raman peak and applying a one-shot, double-potential step (+0.60 to −0.20 V vs. SCE) to the electrode. The RRI vs. time transients for the 1421 and 2194 cm⁻¹ TCNE·⁻ modes for a double potential step duration $\tau = 2.50$ sec are shown in Figure 6. For comparison chronoamperometry and chronoabsorptometry transients obtained under identical experimental conditions are also shown. That these Raman transients correlate exactly in time with the chronoamperometry and chronoabsorptometry signals proves that we are able to monitor TCNE·⁻ in the diffusion layer. The Raman transients also show that the cyclic potential step spectra must be due to TCNE·⁻ in the diffusion layer rather than TCNE·⁻ that has convected out into the bulk of solution. It should be emphasized that the Raman transients in Figure 6 were obtained with the same monochromator bandpass (2–3 cm⁻¹) used to obtain the spectra shown in Figure 5. Considerable improvement in the S/N ratio of these transients can be obtained by opening the slits to the full width at half-maximum height of the Raman bands (ca. 10–15 cm⁻¹). Detailed understanding of the quantitative aspects of the RRI vs. time transients has not yet been fully worked out; however, it is clear from our preliminary studies that self-absorption effects and laser heating induced convection will perturb the shape of these transients. Furthermore multichannel scaling techniques will have to be employed for recording these digital transients in order to avoid time lags due to the ratemeter time constant and to provide the capability for signal averaging. Providing that these effects can be quantitatively accounted for or experimentally eliminated, it appears eminently feasible to use RRI vs. time transients in kinetic studies at least on the time scale of $1.0 < \nu < 10.0$ sec.

The results presented in this first paper on resonance Raman spectroelectrochemistry have been intended to show
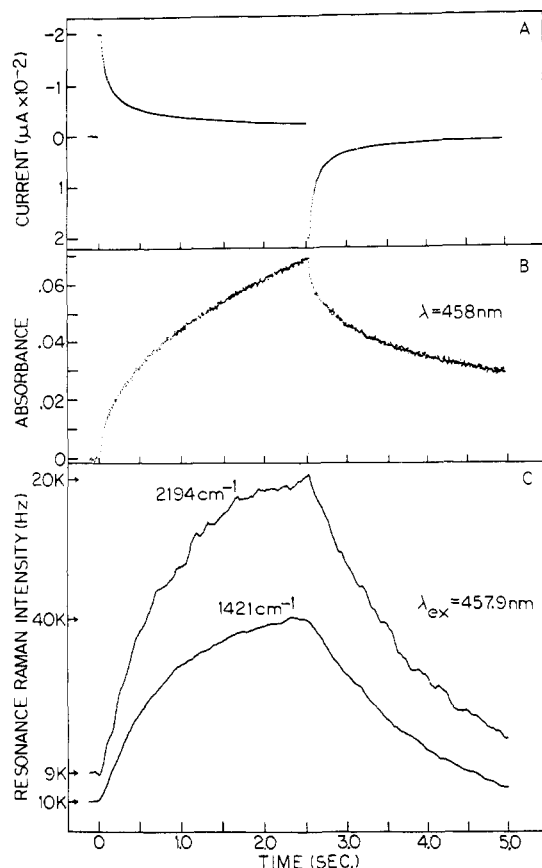
Van Duyne et al. / Resonance Raman Spectroelectrochemistry

1706

Figure 6. TCNE + e⁻ ⇌ TCNE·⁻ transient electrochemical signals during single-shot, double-potential step of 2.5-sec duration from +0.60 V vs. SCE to −0.20 V vs. SCE. (A) Current–time signal at a Pt-OTE; (B) absorbance–time signal at a Pt-OTE; and (C) resonance Raman intensity vs. time signals. The solution contained 3.52 mM TCNE and 0.1 M TBAP in acetonitrile. The ratemeter time constant for the Raman transient was 0.2 sec.

that RRSE offers new possibilities for monitoring the course of electrode reactions and at the same time electrochemical generation provides a readily available source of interesting chemical species for resonance Raman spectroscopy that have electronic absorption bands in the proper location to overlap with conventional laser excitation sources. In particular we would like to emphasize some of the important advantages of resonance Raman spectroscopy as applied to electrochemical problems. For example, in the TCNE·⁻ case, it was possible to observe the C≡N symmetric stretching vibration of a 3×10^{-3} M electrode product in the presence of and totally resolved from the C≡N symmetric stretching vibration of 19 M solvent. The broader absorption lines in IR spectroscopy would not have permitted this resolution. Another important advantage of RRSE with respect to ESR spectroelectrochemistry is that we are not restricted to the observation of paramagnetic electrode products. Thus, for example, we should be able to study Raman frequency shifts throughout the entire electronic structure progression of dication, cation radical, neutral, anion radical, and dianion provided the lifetimes of these species are sufficiently long (ca. 0.1 sec for our present apparatus) and they absorb in an appropriate wavelength region. The restrictiveness of requiring a species to absorb at one of the Ar⁺, Kr⁺, He–Ne, or He–Cd laser lines has, however, been greatly relaxed with the commercial availability of Ar⁺ laser pumped continuous wave dye lasers.

One of the potential problem areas in the development of RRSE is the background fluorescence problem. At the pres-

ent time it would be very difficult if not impossible to observe resonance Raman spectra in an electrochemical system using the cyclic potential step in situ method if the electroactive substrate fluoresced under laser excitation (for example, rubrene). Several possibilities exist to correct this situation such as the use of mode-locked lasers[35] and electrochemical modulation of the Raman signal coupled with digital lock-in detection techniques. Controlled potential electrolysis, on the other hand, could be applied in the case of a fluorescent substrate if one could generate a 100% radical ion solution since it is known that radical ions are efficient fluorescence quenchers[36] as well as exhibiting no luminescence (except in one reported case) themselves.

The future development of RRSE will involve developing other electrogeneration modes (viz., thin layer), development of techniques for recording RRI vs. time transients on the millisecond and microsecond time scales,[37] carrying out isotopic labeling experiments to aid in the fundamental interpretation of the resonance Raman spectra of radical ions and other electrogenerated species,[38] and application to structural and mechanistic investigations. We hope that RRSE will ultimately provide the time scale flexibility for kinetic studies characteristic of uv–visible spectroelectrochemistry, the ability of ESR spectroelectrochemistry to provide positive identification of electrogenerated intermediates, and at the same time be applicable to a wider variety of chemical species.

References and Notes

(1) T. Kuwana, *Ber. Bunsenges. Phys. Chem.*, **77**, 858 (1973), and references therein.
(2) B. Kastening, *Chem. Ing. Tech.*, **42**, 190 (1970).
(3) I. B. Goldberg and A. J. Bard, *J. Phys. Chem.*, **75**, 3281 (1971).
(4) I. B. Goldberg and A. J. Bard, *J. Phys. Chem.*, **78**, 290 (1974).
(5) I. B. Goldberg, D. Boyd, R. Hirasawa, and A. J. Bard, *J. Phys. Chem.*, **78**, 295 (1974).
(6) J. Fajer, D. C. Borg, A. Forman, D. Dolphin, and R. H. Felton, *J. Am. Chem. Soc.*, **92**, 3451 (1970).
(7) P. T. Kissinger and C. N. Reilley, *Anal. Chem.*, **42**, 12 (1970).
(8) J. E. McClure, *Anal. Chem.*, **42**, 551 (1970).
(9) K. Ezumi, H. Miyazaki, and T. Kubota, *J. Phys. Chem.*, **74**, 2397 (1970).
(10) R. E. Dessy and R. L. Pohl, *J. Am. Chem. Soc.*, **90**, 1995 (1968).
(11) H. B. Mark and B. S. Pons, *Anal. Chem.*, **38**, 110 (1966).
(12) D. R. Tallant and D. Evans, *Anal. Chem.*, **41**, 835 (1969).
(13) W. R. Heineman, J. N. Burnett, and R. W. Murray, *Anal. Chem.*, **40**, 1970 (1968).
(14) D. Laser and M. Ariel, *J. Electroanal. Chem.*, **41**, 381 (1973).
(15) M. Fleischmann, P. J. Hendra, and A. J. McQuillan, *J. Chem. Soc., Chem. Commun.*, 80 (1973).
(16) T. Ikesnoji, Y. Ono, and T. Mizuno, *Appl. Opt.*, **12**, 2236 (1973).
(17) M. Fleischmann, P. J. Hendra, and A. J. McQuillan, *Chem. Phys. Lett.*, **26**, 163 (1974).
(18) W. Kiefer and H. J. Bernstein, *Mol. Phys.*, **23**, 835 (1972), and references therein.
(19) R. P. Van Duyne and C. N. Reilley, *Anal. Chem.*, **44**, 142 (1972).
(20) E. R. Brown, D. E. Smith, and G. L. Booman, *Anal. Chem.*, **40**, 1411 (1968).
(21) N. Winograd, H. N. Blount, and T. Kuwana, *J. Phys. Chem.*, **73**, 3456 (1969).
(22) T. Osa and T. Kuwana, *J. Electroanal. Chem.*, **22**, 389 (1969).
(23) R. Nicholson and I. Shain, *Anal. Chem.*, **36**, 706 (1964).
(24) B. J. Huebert and D. E. Smith, *J. Electroanal. Chem.*, **31**, 333 (1971).
(25) W. M. Schwartz and I. Shain, *J. Phys. Chem.*, **69**, 30 (1965).
(26) A. J. Bard and K. S. V. Santhanam, "Electroanalytical Chemistry," Vol. 4, A. J. Bard, Ed., Marcel Dekker, New York, N.Y., 1970, pp 215–315.
(27) E. A. Mayeda and A. J. Bard, *J. Am. Chem. Soc.*, **95**, 6223 (1973).
(28) O. W. Webster, W. Mahler, and R. E. Benson, *J. Am. Chem. Soc.*, **84**, 3678 (1962).
(29) M. Itoh, *J. Am. Chem. Soc.*, **92**, 886, 7239 (1970).
(30) D. F. Shriver and J. B. R. Dunn, *Appl. Spectrosc.*, **28**, 319 (1974).
(31) J. W. Akitt, A. K. Covington, J. F. Freeman, and T. H. Lilley, *Trans. Faraday Soc.*, **65**, 2701 (1969).
(32) R. E. Hester and R. A. Plane, *Inorg. Chem.*, **3**, 769 (1964).

(33) J. J. Hinkel and J. P. Devlin, *J. Chem. Phys.*, **48**, 4750 (1973).
(34) K. Kaya, A. Nakatsuka, N. Kubota, and M. Ito, *J. Raman Spectrosc.*, **1**, 595 (1973).
(35) R. P. Van Duyne, D. L. Jeanmaire, and D. F. Shriver, *Anal. Chem.*, **46**,

213 (1974).
(36) R. P. Van Duyne, *J. Am. Chem. Soc.*, **95**, 7164 (1973).
(37) R. P. Van Duyne and D. L. Jeanmaire, 1974, unpublished results.
(38) R. P. Van Duyne and D. L. Jeanmaire, to be published.

Laser-Induced Fluorescence Studies of Alkali Metal Atom–Carbon Tetrahalide Matrix Reaction Products. Fluorescence Spectra of CBr2 and CClBr in Solid Argon at 15°K

David E. Tevault and Lester Andrews*[1]

Contribution from the Chemistry Department, University of Virginia, Charlottesville, Virginia 22901. Received August 26, 1974

Abstract: CBr_2 and CClBr have been prepared by matrix reactions of alkali metal atoms with the appropriate tetrahalomethanes. Intense red fluorescence spectra from each of these carbenes have been recorded using 5682-Å excitation from a krypton ion laser. Analysis of the CBr_2 fluorescence spectrum observed following metal atom reactions with CBr_4 and $CClBr_3$ in argon gave a value of 196 cm^{-1} for the ground state bending mode. CClBr spectra were produced by metal atom reactions with CCl_2Br_2 in argon and a value of 257 cm^{-1} was determined for the ground state bending mode. Similar reactions of alkali metal atoms with CI_4 have failed to yield a fluorescence spectrum for CI_2.

Infrared spectra of dihalocarbene species have been extensively studied by the matrix-isolation technique. CBr_2, CClBr, and CCl_2 have been produced by alkali metal atom reactions with mixed bromine–chlorine tetrahalomethanes.[2] The latter two carbenes have also been isolated by pyrolysis of the appropriate $C_6H_5HgCX_3$ compound.[3] CF_2 and CCl_2 have been prepared by the reaction of photolytically produced carbon atoms with molecular fluorine and chlorine.[4,5] The infrared spectrum of CFCl was recorded following hard uv photolysis of CH_2FCl during deposition.[6] However, only CF_2 has been produced in sufficient quantity in a matrix environment to directly observe the bending mode, ν_2 at 668 cm^{-1}.[4]

Very recently, the bending modes of CFCl and CCl_2 have been determined from the laser-induced fluorescence spectra of the matrix-isolated species. The blue CFCl fluorescence, excited by near-uv laser lines, exhibited a 445-cm^{-1} spacing which was attributed to ν_2 of CFCl,[7] and the red CCl_2 fluorescence, stimulated by blue-green excitation, displayed as a 326-cm^{-1} interval.[8] Following this trend, CClBr, CBr_2, and CI_2 were expected to have fluorescence spectra excited by green, yellow, and red laser lines. The present report describes the observed CClBr and CBr_2 fluorescence spectra and the attempts to observe CI_2.

Experimental Section

Sample preparation, alkali metal atom, and spectroscopic techniques have been described in detail in previous publications from this laboratory.[7,9,10] CBr_4 (Eastman Organic Chemicals, Reagent) was purified by recrystallization from methanol, $CClBr_3$ was synthesized as described previously,[2a] CCl_2Br_2 (Eastern Chemical Co.) was shaken with elemental mercury to remove bromine impurities, and CCl_3Br (Aldrich, spectroscopic) and CI_4 (K & K Laboratories, Inc.) were used without purification. Lithium-7 (ORNL, 99.99%) and sodium (Baker, lump) were cut, rinsed with hexane, and loaded into the Knudsen cell immediately before the reaction vessel was evacuated. CI_4–argon samples were deposited by passing argon over CI_4 in a Pyrex tube heated to approximately 60°. CBr_4 and $CClBr_3$ matrix samples were prepared by allowing the vapor to equilibrate in a 2-l. can and adding argon gas. CCl_2Br_2 and CCl_3Br samples were prepared using standard manometric techniques.

Fluorescence spectra were recorded at 50 cm^{-1}/min and 1 cm/min chart speed on a Spex Ramalog. Spectra were excited using Coherent Radiation Model 52 G krypton and argon ion lasers and calibrated by superimposing laser emission lines.

Results

A weak red fluorescence spectrum was observed with 4880- and 5145-Å argon ion laser excitation of carbon tetrabromide–alkali metal matrix samples. Krypton ion laser excitation (5309 and 5682 Å) produced a better resolved and more intense fluorescence spectrum, which is shown in Figure 1 for the yellow excitation of a matrix prepared by the reaction of sodium atoms with an Ar–CBr_4 = 1000:1 sample. The most obvious feature of this spectrum is the progression of 17 sharp bands with approximately 196-cm^{-1} spacings, which are labeled *a* in Figure 1 and listed in Table I. Another less-extensive 196-cm^{-1} spaced progression with ten members was also observed with constant relative intensity to the main progression. This progression, which was most prominent at higher quantum numbers, is also listed in Table I and labeled *b* in Figure 1.

Figure 2 shows the fluorescence spectra resulting when alkali metal atom–argon mixed-tetrahalomethane samples were irradiated with 5682-Å krypton ion laser excitation. The top spectrum in this figure, produced following the reaction of $CClBr_3$ with sodium, is identical to that observed when alkali metal atoms were reacted with CBr_4. The bottom scan from the CCl_3Br reaction with sodium is the same spectrum but a factor of 20 weaker than the spectrum produced from alkali metal–CCl_4 and –CCl_3Br matrix samples irradiated with 5145-Å argon ion laser excitation;[8,11] 5682-Å excitation reaches the beginning of the CCl_2 absorption band[5] and, therefore, produces a weaker fluorescence spectrum than 5145 Å, which has a larger absorption coefficient. The bottom spectrum has been assigned to CCl_2 perturbed by another molecule in an adjacent matrix site.[8]

The middle spectrum, recorded with 5682-Å excitation following the matrix reaction of lithium atoms with CCl_2Br_2 in argon, consists of several progressions which are spaced by 257 cm^{-1}. This spacing is intermediate between